Radiotracers to Address Unmet Clinical Needs in Cardiovascular Imaging, Part 2: Inflammation, Fibrosis, Thrombosis, Calcification, and Amyloidosis Imaging

John C. Stendahl*[1], Jennifer M. Kwan*[1], Darko Pucar[2], and Mehran M. Sadeghi[1,3]

[1]Section of Cardiovascular Medicine, Yale University School of Medicine, New Haven, Connecticut; [2]Department of Radiology and Biomedical Imaging, Yale University School of Medicine, New Haven, Connecticut; and [3]Veterans Affairs Connecticut Healthcare System, West Haven, Connecticut

Cardiovascular imaging is evolving in response to systemwide trends toward molecular characterization and personalized therapies. The development of new radiotracers for PET and SPECT imaging is central to addressing the numerous unmet diagnostic needs that relate to these changes. In this 2-part review, we discuss select radiotracers that may help address key unmet clinical diagnostic needs in cardiovascular medicine. Part 1 examined key technical considerations pertaining to cardiovascular radiotracer development and reviewed emerging radiotracers for perfusion and neuronal imaging. Part 2 covers radiotracers for imaging cardiovascular inflammation, thrombosis, fibrosis, calcification, and amyloidosis. These radiotracers have the potential to address several unmet needs related to the risk stratification of atheroma, detection of thrombi, and the diagnosis, characterization, and risk stratification of cardiomyopathies. In the first section, we discuss radiotracers targeting various aspects of inflammatory responses in pathologies such as myocardial infarction, myocarditis, sarcoidosis, atherosclerosis, and vasculitis. In a subsequent section, we discuss radiotracers for the detection of systemic and device-related thrombi, such as those targeting fibrin (e.g., ^{64}Cu-labeled fibrin-binding probe 8). We also cover emerging radiotracers for the imaging of cardiovascular fibrosis, such as those targeting fibroblast activation protein (e.g., ^{68}Ga-fibroblast activation protein inhibitor). Lastly, we briefly review radiotracers for imaging of cardiovascular calcification (^{18}F-NaF) and amyloidosis (e.g., ^{99m}Tc-pyrophosphate and ^{18}F-florbetapir).

Key Words: molecular imaging; fibrosis; inflammation; radiotracers; thrombosis

There is a growing trend in cardiovascular medicine toward molecular characterization and personalized therapies. The development of improved radiotracers for PET and SPECT imaging is central to addressing the clinical needs of the evolving clinical landscape. This 2-part review examines key technical considerations pertaining to cardiovascular radiotracer development and discusses emerging radiotracers in important areas of cardiovascular imaging. Technical considerations and radiotracers for cardiovascular perfusion and neuronal imaging were discussed in part 1. Part 2 covers emerging radiotracers for imaging cardiovascular inflammation, fibrosis, thrombosis, calcification, and amyloidosis (Table 1).

RADIOTRACERS FOR IMAGING CARDIOVASCULAR INFLAMMATION

Inflammation promotes atherosclerosis, mediates cardiomyopathy, and plays central roles in myocarditis and sarcoidosis (*1–3*). In atherosclerosis, enhanced inflammation is considered a marker of plaque vulnerability and can lead to plaque rupture and acute myocardial infarction (MI) (*1*). Myocardial injury promotes both focal and systemic inflammation, where different subsets of immune cells have distinct roles in tissue damage and repair. Early on, the recruitment of neutrophils and inflammatory monocytes (which differentiate into an M1-like proinflammatory phenotype) promotes tissue damage. After the initial phase of injury, tissue repair is supported by the transition to cells with an M2-like, inflammation-resolving phenotype (*4*). Regulatory T cells are critical to this transition (*5*). Accordingly, tissue

TABLE 1
Select Radiotracers for Imaging of Cardiovascular Inflammation, Thrombosis, Fibrosis, Calcification, and Amyloidosis

Application	Radiotracer	Mechanism/target	Status	Reference
Inflammation	^{18}F-FDG	Glucose analog	FDA-approved for myocardial viability imaging	(11,12)
	^{11}C-PK11195	Mitochondrial TSPO	Initial clinical evaluations	(17,18)
	^{11}C-PBR28	TSPO	Initial clinical evaluations	(19,21)
	^{18}F-PBR06	TSPO	Initial clinical evaluations	(19)
	^{18}F-GE180	TSPO	Initial clinical evaluations	(20)
	^{68}Ga-DOTATATE	SSTR	FDA-approved for neuroendocrine tumor imaging	(23)
	^{68}Ga-DOTATOC	SSTR	FDA-approved for neuroendocrine tumor imaging	(26)
	[68]Ga/^{64}Cu-DOTA-ECL1i	CCR2	Initial clinical evaluations	(31,32)
	^{64}Cu-DOTA-vMIP-II	Chemokine receptors (broad)	Preclinical	(33)
	^{68}Ga-pentixafor	CXCR4	Initial clinical evaluations	(30)
	^{99m}Tc-RP805	MMPs	Preclinical	(38)
	^{111}In-RP782	MMPs	Preclinical	(35,36)
	^{99m}Tc-RYM1	MMPs	Preclinical	(38)
	[89]Zr-DFO-anti-CD3	CD3+ T cells	Preclinical	(44)
	[89]Zr-DFO-CD4	CD4+ T cells	Preclinical	(45)
	[89]Zr-DFO-CD8a	CD8+ T cells	Preclinical	(45)
Thrombosis	^{64}Cu-FBP8	Fibrin	Initial clinical evaluations	(49,50)
	^{18}F-GP1	Glycoprotein IIb/IIIa	Initial clinical evaluations	(54,55)
	^{18}F-ENC2015	Factor XIIIa substrate	Preclinical	(58)
Fibrosis	^{68}Ga-FAPI	FAP	Initial clinical evaluations	(67,68)
	^{99m}Tc-collagelin, ^{68}Ga-collagelin	Type I and III collagen	Preclinical	(70,71)
	^{68}Ga-CBP7, ^{68}Ga-CBP8	Type I collagen	Initial clinical evaluations	(72,73)
Calcification	^{18}F-NaF	Hydroxyapatite	FDA-approved for bone imaging	(74–77)
Amyloidosis	^{99m}Tc-pyrophosphate, ^{99m}Tc-HMDP, ^{99m}Tc-DPD	Transthyretin amyloid fibrils	Expanding clinical use*	(82)
	^{11}C-Pittsburgh compound B	Amyloid fibrils (AL, ATTR)	Initial clinical evaluations	(83)
	^{18}F-florbetapir, ^{18}F-flutemetamol, ^{18}F-florbetaben	Amyloid fibrils (AL, ATTR)	FDA-approved for imaging brain β-amyloid plaques	(84–86)

*[99m]Tc-pyrophosphate is FDA-approved for imaging of bone, acute MI, and blood pool.

inflammation plays a dual role after myocardial injury, and dysregulation of this process can lead to cardiomyopathy and heart failure. T lymphocytes also play major roles in autoimmune and viral myocarditis (2), as well as in sarcoidosis, where the secretion of cytokines such as interferon γ is crucial to granuloma formation (6). Chemokines and chemokine receptors, such as chemokine receptor type 2 (CCR2) and CXC chemokine receptor type 4 (CXCR4), mediate the recruitment of monocytes and other inflammatory cells (7). These inflammatory cells are sources of proteases that modulate inflammation and tissue remodeling, including cathepsins and matrix metalloproteases (MMPs) (8,9). Dysregulated protease activation can destabilize atheroma and contribute to adverse myocardial remodeling (8,10).

Cardiovascular inflammation in pathologies such as vasculitis and sarcoidosis has traditionally been imaged with ^{18}F-FDG PET (11,12). ^{18}F-FDG uptake in inflammation is attributed to the high metabolic activity of immune cells, such as macrophages and neutrophils (13,14). One challenge with ^{18}F-FDG PET for imaging of cardiovascular inflammation is its lack of specificity, which, for instance, mandates dietary interventions to suppress myocardial uptake. In addition, ^{18}F-FDG cannot distinguish between subsets of inflammatory cells that characterize the different stages of the

inflammatory process and play distinct roles in cardiovascular disease. Addressing this limitation by targeting more specific molecular signatures may help to better define disease stages, monitor disease progression, guide the selection of therapeutic interventions, and follow responses to treatment. The availability of highly specific tracers, potentially in the setting of multitracer PET and SPECT imaging to fine-tune diagnoses, will be critical for expanded diagnostic and theranostic applications in cardiovascular inflammation. The potential of dual-tracer imaging is illustrated in a recent dual-tracer PET study of patients with ischemic stroke and ipsilateral carotid stenosis, which revealed that uptake of ^{18}F-FDG (inflammation) and ^{18}F-NaF (microcalcification) were both greater in culprit than nonculprit atheroma, although ^{18}F-NaF was concentrated at carotid bifurcations and ^{18}F-FDG was distributed more evenly throughout arteries (Fig. 1) (15). This differential uptake may reflect the distinct roles of inflammation and calcification in plaque development and vulnerability.

Several radiotracers that were initially developed for other applications also bind to target molecules on inflammatory cells and could be of value for imaging cardiovascular inflammation. Radiotracers with preexisting human studies, including those with U.S. Food and Drug Administration (FDA) approval for other indications, expedite the process for testing and potential clinical introduction. Examples of radiotracers potentially useful for imaging cardiovascular inflammation, including some initially developed for other applications, are reviewed in the following sections.
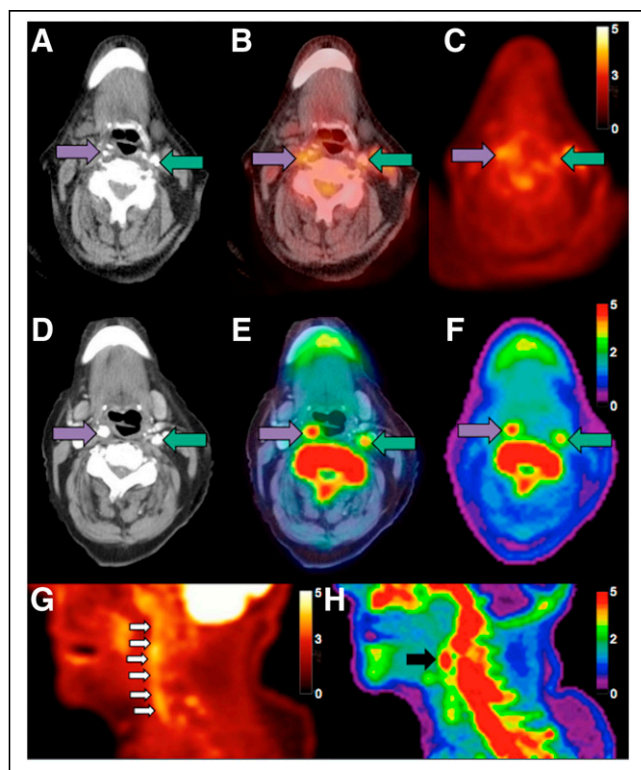

FIGURE 1. Differential distributions of inflammation and microcalcification in symptomatic carotid atheroma. Axial noncontrast CT (A), ^{18}F-FDG PET/CT (B), ^{18}F-FDG PET (C), CT angiography (D), ^{18}F-NaF PET/CT (E), and ^{18}F-NaF PET (F) show symptomatic right carotid artery (purple arrow) and asymptomatic left carotid artery (green arrow); sagittal ^{18}F-FDG PET/CT (G) shows diffuse uptake in symptomatic carotid artery (arrows); and ^{18}F-NaF PET (H) shows focal uptake in symptomatic carotid artery (arrow). (Reprinted from (15).)

Mitochondrial Translocator Protein (TSPO) Imaging

TSPO, a ubiquitous mitochondrial protein involved in a large number of cellular functions, including mitochondrial cholesterol transport and steroid hormone biosynthesis (16), is classically used as a marker of neuroinflammation. More recently, expression of TSPO in activated macrophages has motivated the evaluation of radiotracers targeting TSPO for imaging of cardiovascular inflammation in pathologies such as MI, myocarditis, sarcoidosis, atherosclerosis, and vasculitis. Examples of such radiotracers include 1-[2-chlorophenyl]-N-methyl-N-[1-methyl-propyl]-3-isoquinoline carboxamide (^{11}C-PK11195) (17,18), N-acetyl-N-(2-^{11}C-methoxybenzyl)-2-phenoxy-5-pyridinamine (^{11}C-PBR28) (19), ^{18}F-N-fluoroacetyl-N-(2,5-dimethoxybenzyl)-2-phenoxyaniline (^{18}F-PBR06) (19), and ^{18}F-flutriciclamide (^{18}F-GE180) (20). The prototypic TSPO tracer ^{11}C-PK11195 has been evaluated for the detection of inflammation in human carotid atherosclerotic plaques, where plaques associated with recent ipsilateral stroke or transient ischemic attack were shown to have greater ^{11}C-PK11195 uptake than those without a recent event (target-to-background ratio, 1.06 ± 0.20 vs. 0.86 ± 0.11, $P = 0.001$) (17). Plaques associated with stroke or transient ischemic attack also had lower CT attenuation, but there was no correlation between ^{11}C-PK11195 target-to-background ratio and CT plaque attenuation. Importantly, the combination of these 2 features had 100% sensitivity and a 100% positive predictive value in identifying patients with recent stroke or transient ischemic attack. Although these results are promising, it is not known whether the same approach can be used to identify the plaques at risk for future events. ^{11}C-PK11195 PET has also demonstrated increased uptake in patients with large-vessel vasculitis (Fig. 2) (18). However, in another study of patients with stroke or vasculitis, other TSPO tracers (^{11}C-PBR28 and ^{18}F-PBR06) did not produce significant in vivo signals (19). Of note, there is also considerable uptake of ^{11}C-PBR28 in normal myocardium (21), which may limit its utility for imaging of cardiac inflammation.

Another TSPO-targeting tracer, ^{18}F-GE180, has shown greater binding to M1-polarized macrophages than M2-polarized macrophages (20). In a murine study of MI, an early increase in ^{18}F-GE180 uptake was observed at the site of infarct, with signals returning to the reference range after 4 wk, suggesting that the TSPO signal may reflect early post-MI inflammation (20). Importantly, global ^{18}F-GE180 uptake at 1 wk predicted a future reduction in left ventricular ejection fraction. Small-scale human studies have confirmed the early increase in post-MI ^{18}F-GE180 signal (20), and additional clinical studies are being conducted to evaluate this tracer for imaging cardiac sarcoidosis (NCT03561025). Unresolved issues regarding TSPO-targeted imaging of cardiovascular inflammation include noninflammatory cell expression of TSPO, the selectivity of the
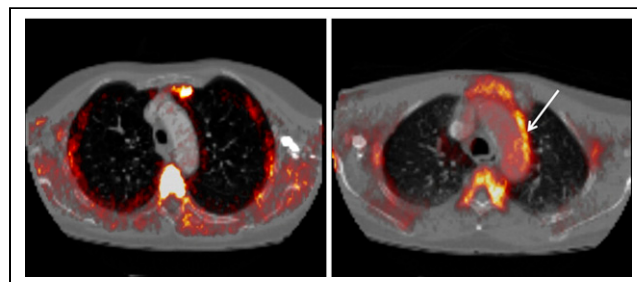
FIGURE 2. ^{11}C-PK11195 PET imaging of large-vessel vasculitis in patients with systemic inflammatory disorders. ^{11}C-PK11195 PET images fused with CT angiograms demonstrate minimal radiotracer uptake in asymptomatic patient (A) and elevated uptake in symptomatic patient (B). Arrow indicates inflamed region of aortic arch. (Reprinted from (18).)

tracers for different TSPO isoforms and multimers, and whether the magnitude of radiotracer signals is sufficient for clinical applications. In addition, interpretation of human studies is affected by a genetic polymorphism that influences tissue binding of certain TSPO radiotracers (22). Addressing these limitations will be necessary for routine use of TSPO-targeted imaging in clinical cardiovascular medicine.

Somatostatin Receptor (SSTR) Imaging

SSTR-targeted radiotracers have been classically used as neuroendocrine tumor imaging agents. There are 5 subtypes of SSTRs, with peripheral blood mononuclear cells expressing mainly SSTR subtypes 2 and 3. Macrophages mainly express SSTR subtype 2, with the highest expression detected in inflammatory M1 macrophages (23), whereas lymphocytes express mainly SSTR subtype 3 (24). There are important variations in receptor subtype affinity profiles between different SSTR-targeted tracers (25). The ^{68}Ga-labeled somatostatin analog ^{68}Ga-DOTATATE binds to SSTR2 with high affinity and selectivity relative to other SSTRs (25). In a prospective study of patients with cardiovascular disease, ^{68}Ga-DOTATATE uptake in atherosclerotic plaques was shown to be macrophage-specific and discriminate between culprit and nonculprit plaques in patients with acute coronary syndrome and cerebrovascular accidents (23). Furthermore, the ^{68}Ga-DOTATATE signal in plaques was associated with high-risk coronary CT features (e.g., spotty calcification, low attenuation, positive remodeling) and correlated with Framingham risk score ($r = 0.53$, $P < 0.0001$) and ^{18}F-FDG uptake ($r = 0.73$, $P < 0.0001$) (23). In a separate study of sarcoidosis patients, PET imaging with ^{68}Ga-DOTATOC, which has a high affinity for SSTR2 and moderate affinity for SSTR5, performed better than conventional ^{67}Ga-scintigraphy for the detection of sarcoidosis lesions (26). However, whereas basal uptake of ^{68}Ga-DOTATOC in the heart was minimal, none of the patients in the study had active cardiac sarcoidosis. As such, additional information is needed to establish the value of SSTR2-targeted radiotracers for imaging of cardiovascular inflammation. In this regard, potential impediments to clinical applications of ^{68}Ga-DOTATATE for imaging of cardiovascular inflammation include the modest level of increase in SSTR2 expression in culprit atherosclerotic plaques (23).

Chemokine Receptor Imaging

Chemokines are a family of small chemoattractant proteins that play key roles in leukocyte recruitment and activation through binding to chemokine receptors. Radiotracers that target chemokine receptors such as CXCR4 and CCR2 have recently emerged as promising agents for imaging inflammation (27,28). ^{68}Ga-pentixafor was initially developed for CXCR4 imaging in cancer (29). Recent studies on mice have shown that post-MI ^{68}Ga-pentixafor uptake is increased in parallel with leukocyte infiltration (30). In patients with acute MI, PET imaging showed variable patterns of ^{68}Ga-pentixafor uptake (30). Furthermore, whereas there was no correlation with summed rest perfusion defect score, late gadolinium enhancement, or edema score by MRI, the ^{68}Ga-pentixafor signal correlated with a combination of infarct size and time of imaging after reperfusion ($r_{multiple} = 0.73$, $P = 0.03$) (30). Examples of other radiotracers that target chemokine receptors include [68]Ga- and ^{64}Cu-DOTA-ECL1i (31,32), which target CCR2, and ^{64}Cu-viral macrophage inflammatory protein-II (^{64}Cu-DOTA-vMIP-II), which targets a broad range of chemokine receptors (33). CCR2 is upregulated on inflammatory cells after myocardial injury (34) and in abdominal aortic aneurysms (AAAs) (32). CCR2-targeted imaging with ^{64}Cu-DOTA-ECL1i is undergoing clinical evaluation in patients with AAAs (NCT04592991). This study follows

promising results with ECL1i-based tracers in rodent studies that established the ability to detect CCR2+ monocytes and macrophages within post-MI hearts (^{68}Ga-DOTA-ECL1i) (31) and demonstrated greater radiotracer uptake in AAAs that subsequently ruptured (^{64}Cu-DOTA-ECL1i) (32).

MMP Imaging

Inflammatory cells are a major source of proteases, and MMP activation contributes to atherosclerotic plaque vulnerability, adverse left ventricular remodeling after MI, and AAA development and rupture. MMP-targeted radiotracers that target a broad range of MMPs, including ^{111}In-RP782, ^{99m}Tc-RP805, and ^{99m}Tc-RYM1, have shown promise in preclinical studies of post-MI remodeling, atherosclerosis, calcific aortic valve disease, and aortic aneurysms (35–40). Tissue uptake of these tracers correlates well with both MMP activity and CD68 macrophage expression in murine models of atherosclerosis (35,41), calcific aortic valve disease (39), and aneurysm (40). Accordingly, MMP-targeted imaging may indirectly inform on the extent of cardiovascular inflammation. For instance, in a murine model of angiotensin-II–induced AAA, aortic ^{99m}Tc-RP805 signals on small-animal SPECT/CT images correlated with MMP activity quantified by zymography ($r = 0.83$, $P < 0.001$), as well as CD68 messenger RNA expression, a marker of monocytes and macrophages ($r = 0.89$, $P < 0.0001$) (40). Importantly, the MMP signal at 1 wk after angiotensin-II infusion correlated with AAA size at 4 wk ($r = 0.53$, $P < 0.01$), highlighting the potential of MMP-targeted imaging for AAA risk stratification. ^{99m}Tc-RYM1, which has a fast blood clearance, allows for imaging at 1 h after tracer injection and can similarly detect aortic MMP activity in murine models of aneurysm (Fig. 3) (38). Clinical studies with these MMP-targeted radiotracers are expected soon. The relative effectiveness of these broad-spectrum tracers as compared with emerging tracers that target specific members of the MMP family (e.g., MMP-12) remains to be determined (42).

T-Cell Imaging

Different lymphocyte subsets play distinct roles in inflammation. For instance, CD4+ T lymphocytes can activate and recruit other immune cells, whereas CD8+ T cells can mediate cell killing via release of intracellular granzymes (43). Several novel radiotracers that are in early stages of development for oncologic applications can potentially detect T-cell infiltration and may be valuable in cardiovascular applications such as myocarditis or sarcoidosis. Examples of these radiotracers include [89]Zr-desferrioxamine (DFO)-anti-CD3, which targets all types of T cells (44), [89]Zr-DFO-CD4 (45), and [89]Zr-DFO-CD8a (45). Future studies should address the value of these and related imaging agents in the diagnosis and management of inflammatory cardiovascular disease.

RADIOTRACERS FOR THROMBOSIS IMAGING

Thrombosis plays a central role in the pathogenesis of multiple disabling diseases, including MI, stroke, and pulmonary embolism. Detection and localization of the primary thrombus and any secondary emboli are often critically important for diagnosis and treatment. As such, there has been considerable interest in the development of nuclear imaging techniques that could potentially provide sensitive and specific whole-body detection of thrombi.

Fibrin Imaging

Fibrin is the end-product of the coagulation cascade and is one of the most widely pursued targets of radiotracers for thrombus
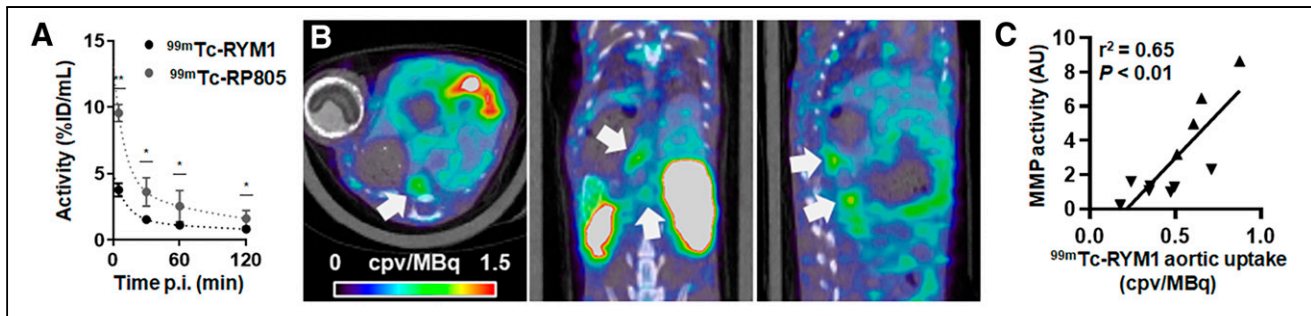
FIGURE 3. ^{99m}Tc-RYM1 imaging of AAA. (A) Comparison of blood clearance of ^{99m}Tc-RYM1 and ^{99m}Tc-RP805 in mice. (B) Examples of fused ^{99m}Tc-RYM1 SPECT/CT images of AAA in angiotensin II–infused mice at 4 wk after aneurysm induction. Arrows point to tracer uptake in AAA on axial (left), coronal (middle), and sagittal (right) views. (C) Aortic ^{99m}Tc-RYM1 signal in vivo correlates well with MMP activity quantified by ex vivo zymography. %ID = percentage injected dose; AU = arbitrary units; cpv = counts per voxel; p.i. = after injection. (Reprinted from (*38*).)

imaging (*46*). As fibrin is present in developing and mature thrombi, and absent from circulating blood, specific detection relies on target-selective binding to distinguish it from fibrinogen, its similar, widely circulating precursor (*46*). Early fibrin-targeted molecular diagnostic procedures were performed with radiolabeled fibrinogen and later with radiolabeled antifibrin antibodies and antibody fragments. However, the field has since moved in the direction of fibrin-binding peptides, given their generally more favorable production, binding, and pharmacokinetic characteristics. Numerous fibrin-binding peptides have been developed and labeled for MR, PET, PET/MR, and SPECT imaging in preclinical thrombosis models (*46–48*). One such fibrin-targeted PET radiotracer, ^{64}Cu-labeled fibrin-binding probe 8 (^{64}Cu-FBP8), demonstrated highly accurate carotid artery and femoral vein thrombus detection in rats (97.6%; 95% CI, 92–100) (*49*). Moreover, the ^{64}Cu-FBP8 signal provided insight into clot chronicity and composition, as ^{64}Cu-FBP8 uptake was greater in younger than older clots in both arteries and veins. This result was corroborated by quantitative histopathology, which demonstrated an age-dependent reduction in thrombus fibrin content. ^{64}Cu-FBP8 is undergoing clinical investigation to evaluate its effectiveness for left atrial appendage thrombus imaging (NCT03830320) (*50*). Initial results demonstrated that ^{64}Cu-FBP8 is metabolically stable and undergoes rapid bloodstream clearance. In addition, maximum SUVs in left atrial appendages were significantly greater in patients with transesophageal imaging–confirmed left atrial appendage thrombi than those with negative imaging results (median, 4.0 [interquartile range, 3.0–6.0] vs. median, 2.3 [interquartile range, 2.1–2.5]; $P < 0.001$). ^{64}Cu-FBP8 is also being evaluated clinically for the detection of deep venous thrombosis and pulmonary embolism (NCT04022915).

Activated Platelet Imaging

Similar to fibrin, activated platelets are essentially present in large numbers only in developing thrombi and healing wounds and are thus attractive targets for acute thrombus imaging. The most common target on activated platelets is glycoprotein IIb/IIIa, a heterodimeric membrane receptor that, when activated, binds to von Willebrand factor and to its primary ligand, fibrinogen, to mediate platelet adhesion and aggregation (*51*). ^{99m}Tc-apcitide is an early SPECT imaging agent targeting glycoprotein IIb/IIIa that was approved by the FDA for detection of acute deep venous thrombosis. However, enthusiasm was ultimately tempered by the fact that it was not particularly effective for detecting pulmonary embolism (*52*). ^{18}F-glycoprotein 1 (GP1) is an ^{18}F-labeled derivative of the small-molecule glycoprotein IIb/IIIa antagonist

elarofiban (*53–55*). The binding of ^{18}F-GP1 to glycoprotein IIb/IIIa is highly specific and appears to be minimally affected by aspirin or heparin treatment (*55*). In preliminary clinical evaluations, ^{18}F-GP1 demonstrated the ability to identify thrombotic lesions in patients with acute deep venous thrombosis or pulmonary embolism (*53*), acute arterial thrombi (*54*), bioprosthetic valve thrombi (*56*), left atrial appendage thrombi (*56*), jugular vein thrombi (*56*), and left ventricular assist device thrombi (Fig. 4) (*56*). However, ^{18}F-GP1's vessel-level detection rate of pulmonary embolism was significantly lower than that for deep venous thrombosis (60% vs. 89%, $P < 0.001$), a finding that may relate to lower levels of activated platelets in older, embolic thrombi or inhibition of platelet activation in the setting of large pulmonary embolism (*53*). Further evaluation of ^{18}F-GP1 in various clinical settings, including acute deep venous thrombosis (NCT04156230) and bioprosthetic valve thrombosis (NCT04073875), is in progress.

Factor XIIIa Imaging

Factor XIIIa is an activated enzyme that crosslinks fibrin during the terminal step of the coagulation pathway and is thus another molecular target for imaging of thrombosis (*57*). Several factor XIIIa–targeted radiotracers based on α_2-antiplasmin, a substrate of factor XIIIa in the transglutaminase crosslinking reaction, have been evaluated in preclinical models. ^{18}F-ENC2015 is a fluorescent and positron-emitting factor XIIIa-targeting probe that has demonstrated rapid, selective binding to thrombi in initial preclinical carotid artery thrombosis models (*58*). Ultimately, information on the sensitivity of ENC2015 and other tracers to small foci of thrombosis, their effectiveness in the presence of antiplatelet and anticoagulant agents, and their ability to differentiate between active and chronic thrombi will be key to their acceptance as clinical tools.

RADIOTRACERS FOR CARDIOVASCULAR FIBROSIS IMAGING

Tissue fibrosis is a consequence of dysregulated repair responses to various types of injury. Excessive extracellular matrix deposition (mainly collagen) leading to interstitial or replacement fibrosis is the result of dysregulated fibroblast activation and myofibroblast transformation. Inflammation, activation of transforming growth factor β, focal secretion of other cytokines, and MMP activation drive this process (*59*). In the myocardium, fibrosis can lead to cardiac dysfunction and serve as a nidus for arrhythmias (*60*). The burden of myocardial fibrosis related to nonischemic cardiomyopathy and myocardial injuries from MI, cytotoxic chemotherapy or radiation, and inflammatory or immune-mediated conditions (e.g., myocarditis) has
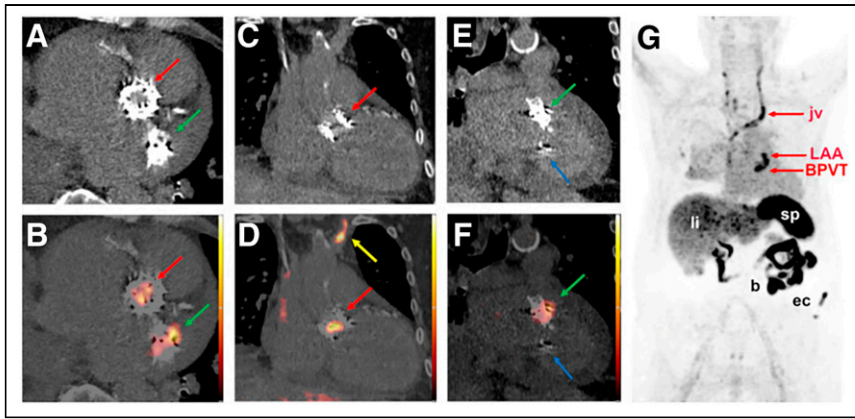
FIGURE 4. Thrombus detection via ^{18}F-GP1 PET/CT. (A–F) Axial (A and B), coronal (C and D), and parasagittal (E and F) unenhanced CT (top) and corresponding ^{18}F-GP1 PET/CT images (bottom) demonstrating bioprosthetic valve (BPVT), left atrial appendage (LAA), and left jugular vein thromboses (jv). (G) Anterior maximum-intensity-projection ^{18}F-GP1 PET image showing distribution of tracer in this patient. (Reprinted from (56).)

prognostic value for cardiovascular outcomes (61,62). Fibrosis also plays a key role in the pathogenesis of vascular diseases such as atherosclerosis (63). Given the association between fibrous cap thickness and vulnerability to plaque rupture, the evaluation of collagen content in atherosclerotic plaques may inform on plaque stability. However, the spatial resolution of current nuclear imaging modalities and the presence of fibrosis elsewhere within the vessel wall are major impediments to this approach.

Classic nuclear cardiology studies such as myocardial perfusion imaging and viability testing allow for indirect assessment of cardiac fibrosis through detection of scar tissue. Measurement of delayed gadolinium enhancement by MRI is another means of assessing myocardial fibrosis. However, these techniques are not sufficiently sensitive for detecting early stages of fibrosis and cannot distinguish between active fibrosis (fibrogenesis) and stable fibrosis or scar. In addition, they provide no information on collagen turnover, which is a target of emerging therapeutic interventions to treat fibrosis (64). Molecular imaging may provide a noninvasive means to monitor and quantify the presence of active fibrosis and determine the efficacy of therapeutics targeting fibrotic processes.

Fibroblast Activation Protein (FAP) Imaging

FAP, a type II transmembrane glycoprotein with collagenase activity, has recently emerged as a promising target for fibrogenesis imaging. This marker of fibroblast activation is not detectable in most healthy adult tissues but can be upregulated in pathologic states such as cancer, atherosclerosis, arthritis, and tissue fibrosis (65). FAP's overexpression in human tumors and documented role in promoting tumor growth in animal models have led to its evaluation as a diagnostic and therapeutic target in ongoing oncologic clinical trials (NCT04147494 and NCT04554719). In parallel, FAP-targeted tracers are emerging as potential tools for imaging fibroblast activation and fibrosis in other settings, such as cardiovascular disease. ^{68}Ga-FAP inhibitor (FAPI)–04 PET imaging in a rodent model of MI has shown significantly increased tracer uptake in injured myocardium 6 d after coronary ligation, with immunohistochemistry and autoradiography demonstrating that the PET signals corresponded to FAP-positive myofibroblasts concentrated in the infarct border zones (66). Cardiac expression of FAP has also been studied indirectly in cancer patients undergoing ^{68}Ga-FAPI PET imaging. In one study, left ventricular uptake of ^{68}Ga-FAPI

correlated strongly with reduced ejection fraction by univariate analysis ($r^2 = 0.74$, $P < 0.01$) and had weaker, but significant, correlations with age ($r^2 = 0.15$, $P = 0.04$) and the presence of coronary artery disease ($r^2 = 0.16$, $P = 0.03$) (Fig. 5) (67). Another study demonstrated that left ventricular ^{68}Ga-FAPI uptake correlated with the presence of cardiovascular risk factors such as overweight status (odds ratio, 2.6; $P = 0.023$), type 2 diabetes (odds ratio, 2.9; $P = 0.041$), and histories of platinum-based chemotherapy (odds ratio, 3.0; $P = 0.034$) and chest radiation (odds ratio, 3.5; $P = 0.024$) (68). Finally, a retrospective analysis of ^{68}Ga-FAPI PET/CT images obtained for noncardiovascular indications showed that focal arterial uptake of the tracer correlated negatively with calcification ($r = -0.27$, $P < 0.01$) (69). Several ongoing clinical trials seek to establish the role of FAPI imaging to detect post-MI cardiac fibrosis (NCT04803864, NCT04723953).

Extracellular Matrix Imaging

Collagens, especially types I and III, constitute the bulk of fibrotic tissue and accordingly have been used as targets for imaging of fibrosis. Several SPECT and PET tracers that target different types of collagen, including ^{99m}Tc-collagelin (70), ^{68}Ga-collagelin (71), ^{64}Cu-collagen-binding probe (CBP) 7 (72), and ^{64}Cu-CBP8 (73), have been used in animal and human studies to evaluate fibrosis. However, there are only a few reports of using these tracers in the cardiovascular system. For instance, in a rat model of MI, ^{99m}Tc-collagelin tracer uptake occurred in areas of histologically confirmed fibrosis (70). Additional studies are needed to establish the utility of these radiotracers for cardiovascular fibrosis imaging. Given the role of MMPs in extracellular matrix remodeling, MMP-targeted imaging may also provide valuable information on fibrotic processes in cardiovascular disease.

^{18}F-NAF PET IMAGING OF CARDIOVASCULAR CALCIFICATION

Ectopic calcification in arteries and cardiac valves is driven by osteoblastic differentiation of vascular smooth muscle cells and valvular interstitial cells. The role of calcification in cardiovascular
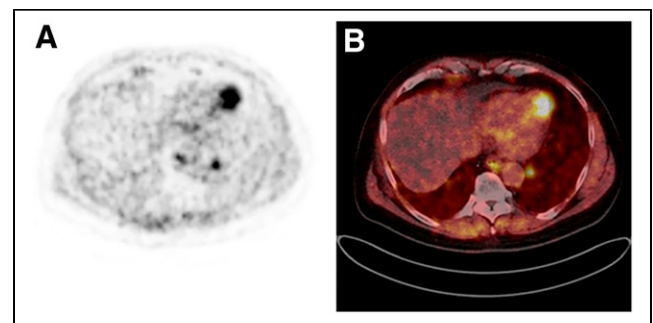
FIGURE 5. Detection of cardiac fibroblast activation via ^{68}Ga-FAPI PET/CT. Transaxial images of ^{68}Ga-FAPI PET (A) and ^{68}Ga-FAPI PET/CT (B) demonstrate left ventricular radiotracer uptake in patient with papillary thyroid cancer. (Reprinted from (67).)

pathology is complex and context-dependent. In coronary arteries, microcalcification is considered a classic feature of vulnerable plaque that is prone to rupture, whereas macrocalcification may be associated with plaque stability (74). In valvular disease, calcification directly contributes to the development of valvular dysfunction. Accordingly, there is potential value in detecting calcification as a diagnostic and possibly prognostic tool in cardiovascular disease. Although CT can detect established, macroscopic foci of calcification, ^{18}F-NaF PET has recently emerged as a promising tool to detect the process of calcification. Fluoride binds to hydroxyapatite in calcified tissue through an exchange process with hydroxyl groups. Microcalcifications have greater surface area per mass for ^{18}F-NaF binding than do macrocalcifications and thus tend to produce more intense signals (74). Recent studies have shown greater uptake of ^{18}F-NaF in culprit plaques after recent acute coronary syndrome (75), and a post hoc analysis of several observational studies showed that global estimates of coronary ^{18}F-NaF signals in patients with known coronary artery disease may predict future risks of MI (76). Ongoing studies such as the Prediction of Recurrent Events with ^{18}F-Fluoride (PREFFIR, NCT02278211) should further clarify the role of ^{18}F-NaF PET imaging in determining risk for future cardiovascular events.

^{18}F-NaF PET has also demonstrated potential clinical utility for imaging of valvular calcification. In patients with calcific aortic valve stenosis and mitral annular calcification, valvular ^{18}F-NaF PET signals have been shown to correlate with the severity of calcification detected by CT. Moreover, ^{18}F-NaF PET signals on valves have been shown to predict the development of macroscopic calcification several years before detection on CT (77–79), and greater ^{18}F-NaF PET signals have been linked to faster progression of calcification, although not independently of baseline CT-derived calcium scoring (77). Several recent comprehensive reviews provide more detailed discussions of the potential of ^{18}F-NaF PET for studying cardiovascular pathophysiology and assessing vascular (carotid and coronary artery atherosclerosis, abdominal aortic aneurism) and valvular diseases and their responses to therapy (80,81).

RADIOTRACERS FOR CARDIAC AMYLOIDOSIS IMAGING

Amyloidosis affects multiple organ systems through extracellular accumulation of amyloid fibrils. These insoluble fibrils form as the result of misfolding and aggregation of various precursor proteins, many of which are normal constituents of plasma. Cardiac involvement is common in the 2 most prevalent forms of amyloidosis, transthyretin amyloidosis (ATTR) and immunoglobulin light-chain amyloidosis (AL). Nuclear imaging has emerged to play a key role in the diagnosis of ATTR and AL cardiomyopathies. Early and accurate detection of these conditions is important given the availability of effective but time-sensitive treatments.

ATTR cardiomyopathy can be diagnosed noninvasively through semiquantitative analysis of planar or SPECT images using ^{99m}Tc-labeled bisphosphonate derivatives that were initially developed for bone imaging. ^{99m}Tc-pyrophosphate is used most in the United States, whereas ^{99m}Tc-hydroxymethylene diphosphonate (^{99m}Tc-HMDP) and ^{99m}Tc-3,3-diphosphono-1,2-propanodicarboxylic acid (^{99m}Tc-DPD) are more commonly used in Europe. These radiotracers are generally considered to have similar diagnostic performance, although direct comparisons are limited. In a multicenter study of patients with suspected amyloid cardiomyopathy, pooled scintigraphy data using these 3 radiotracers demonstrated that the presence of myocardial radiotracer uptake was more than 99%

sensitive and 86% specific for histologically confirmed ATTR, with false-positives related almost exclusively to low-level uptake in the setting of AL (82). Notably, the combination of grade 2 and 3 scintigraphic uptake and negative urine or serum monoclonal protein analysis had a specificity and positive predictive value for ATTR of 100%.

PET radiotracers that were initially developed for imaging of brain amyloid plaques related to Alzheimer disease have been evaluated for the detection of cardiac amyloidosis. In initial studies, ^{11}C-Pittsburgh compound B (83), ^{18}F-florbetapir (84), and ^{18}F-florbetaben (85) have demonstrated potential diagnostic utility for detecting both AL and ATTR cardiomyopathies. ^{18}F-flutemetamol, an ^{18}F-based analog of ^{11}C-Pittsburgh compound B, has also been studied for cardiac amyloid imaging, although more recent work has raised questions about its sensitivity (86). ^{18}F-florbetapir and ^{18}F-florbetaben are currently undergoing evaluation in clinical trials. In all, quantitative PET-based approaches for imaging cardiac amyloidosis may provide additional benefits beyond diagnosis, such as correlating amyloid burden with prognosis (83) or responses to novel disease-modifying treatments (85). Because of the short half-life of ^{11}C, which restricts its use to centers with on-site cyclotrons, ^{18}F-based agents have greater potential for large-scale clinical use.

CONCLUSIONS AND FUTURE PERSPECTIVES

Molecular imaging is anticipated to play an increasingly more prominent role in clinical cardiovascular medicine. Although many radiotracers with potential cardiovascular applications have been evaluated in preclinical and clinical studies, only a select few to date have advanced to mainstream clinical usage. Aside from the technical and performance-related requirements of radiotracer development, clinical implementation requires clear definition of their diagnostic roles and demonstration of added value beyond existing clinical imaging techniques. Moreover, the clinical market for emerging radiotracers must be large enough to justify their initial research and development costs, an issue that may be addressed by targeting key, common biologic processes rather than specific diseases. Although these factors seemingly pose formidable barriers, the demand for new radiotracers is increasing because of evolving trends in medicine toward molecular characterization and personalized therapies. Technical advances in areas such as radiotracer chemistry, instrumentation, and data analysis are facilitating radiotracer development to address the numerous unmet clinical needs.

REFERENCES

1. Soehnlein O, Libby P. Targeting inflammation in atherosclerosis: from experimental insights to the clinic. *Nat Rev Drug Discov.* 2021;20:589–610.
2. Tschöpe C, Ammirati E, Bozkurt B, et al. Myocarditis and inflammatory cardiomyopathy: current evidence and future directions. *Nat Rev Cardiol.* 2021;18:169–193.
3. Murphy SP, Kakkar R, McCarthy CP, Januzzi JL Jr. Inflammation in heart failure: JACC state-of-the-art review. *J Am Coll Cardiol.* 2020;75:1324–1340.
4. Nahrendorf M, Frantz S, Swirski FK, et al. Imaging systemic inflammatory networks in ischemic heart disease. *J Am Coll Cardiol.* 2015;65:1583–1591.
5. Weirather J, Hofmann UD, Beyersdorf N, et al. Foxp3+ CD4+ T cells improve healing after myocardial infarction by modulating monocyte/macrophage differentiation. *Circ Res.* 2014;115:55–67.
6. Grunewald J, Eklund A. Role of CD4+ T cells in sarcoidosis. *Proc Am Thorac Soc.* 2007;4:461–464.
7. Hughes CE, Nibbs RJB. A guide to chemokines and their receptors. *FEBS J.* 2018; 285:2944–2971.
8. Lindsey ML. Assigning matrix metalloproteinase roles in ischaemic cardiac remodelling. *Nat Rev Cardiol.* 2018;15:471–479.

9. Liu CL, Guo J, Zhang X, Sukhova GK, Libby P, Shi GP. Cysteine protease cathepsins in cardiovascular disease: from basic research to clinical trials. *Nat Rev Cardiol.* 2018;15:351–370.

10. Newby AC. Proteinases and plaque rupture: unblocking the road to translation. *Curr Opin Lipidol.* 2014;25:358–366.

11. Slart RH. FDG-PET/CT(A) imaging in large vessel vasculitis and polymyalgia rheumatica: joint procedural recommendation of the EANM, SNMMI, and the PET Interest Group (PIG), and endorsed by the ASNC. *Eur J Nucl Med Mol Imaging.* 2018;45:1250–1269.

12. Chareonthaitawee P, Beanlands RS, Chen W, et al. Joint SNMMI-ASNC expert consensus document on the role of ^{18}F-FDG PET/CT in cardiac sarcoid detection and therapy monitoring. *J Nucl Med.* 2017;58:1341–1353.

13. Tavakoli S, Zamora D, Ullevig S, Asmis R. Bioenergetic profiles diverge during macrophage polarization: implications for the interpretation of ^{18}F-FDG PET imaging of atherosclerosis. *J Nucl Med.* 2013;54:1661–1667.

14. Chen DL, Schuster DP. Positron emission tomography with [^{18}F]fluorodeoxyglucose to evaluate neutrophil kinetics during acute lung injury. *Am J Physiol Lung Cell Mol Physiol.* 2004;286:L834–L840.

15. Evans NR, Tarkin JM, Chowdhury MM, et al. Dual-tracer positron-emission tomography for identification of culprit carotid plaques and pathophysiology in vivo. *Circ Cardiovasc Imaging.* 2020;13:e009539.

16. Ilkan Z, Akar FG. The mitochondrial translocator protein and the emerging link between oxidative stress and arrhythmias in the diabetic heart. *Front Physiol.* 2018;9:1518.

17. Gaemperli O, Shalhoub J, Owen DR, et al. Imaging intraplaque inflammation in carotid atherosclerosis with ^{11}C-PK11195 positron emission tomography/computed tomography. *Eur Heart J.* 2012;33:1902–1910.

18. Lamare F, Hinz R, Gaemperli O, et al. Detection and quantification of large-vessel inflammation with ^{11}C-(R)-PK11195 PET/CT. *J Nucl Med.* 2011;52:33–39.

19. Schollhammer R, Lepreux S, Barthe N, et al. In vitro and pilot in vivo imaging of 18 kDa translocator protein (TSPO) in inflammatory vascular disease. *EJNMMI Res.* 2021;11:45.

20. Thackeray JT, Hupe HC, Wang Y, et al. Myocardial inflammation predicts remodeling and neuroinflammation after myocardial infarction. *J Am Coll Cardiol.* 2018; 71:263–275.

21. Toczek J, Kukreja G, Zhang J, et al. TSPO-targeted PET imaging in aging heart [abstract]. *J Nucl Cardiol.* 2020:1866.

22. Yoder KK, Nho K, Risacher SL, Kim S, Shen L, Saykin AJ. Influence of TSPO genotype on ^{11}C-PBR28 standardized uptake values. *J Nucl Med.* 2013;54:1320–1322.

23. Tarkin JM, Joshi FR, Evans NR, et al. Detection of atherosclerotic inflammation by ^{68}Ga-DOTATATE PET compared to [^{18}F]FDG PET imaging. *J Am Coll Cardiol.* 2017;69:1774–1791.

24. Lichtenauer-Kaligis EG, Dalm VA, Oomen SP, et al. Differential expression of somatostatin receptor subtypes in human peripheral blood mononuclear cell subsets. *Eur J Endocrinol.* 2004;150:565–577.

25. Pauwels E, Cleeren F, Bormans G, Deroose CM. Somatostatin receptor PET ligands: the next generation for clinical practice. *Am J Nucl Med Mol Imaging.* 2018;8:311–331.

26. Nobashi T, Nakamoto Y, Kubo T, et al. The utility of PET/CT with ^{68}Ga-DOTATOC in sarcoidosis: comparison with ^{67}Ga-scintigraphy. *Ann Nucl Med.* 2016;30:544–552.

27. Kircher M, Tran-Gia J, Kemmer L, et al. Imaging inflammation in atherosclerosis with CXCR4-directed ^{68}Ga-pentixafor PET/CT: correlation with ^{18}F-FDG PET/CT. *J Nucl Med.* 2020;61:751–756.

28. Heo GS, Bajpai G, Li W, et al. Targeted PET imaging of chemokine receptor 2-positive monocytes and macrophages in the injured heart. *J Nucl Med.* 2021;62:111–114.

29. Herrmann K, Lapa C, Wester HJ, et al. Biodistribution and radiation dosimetry for the chemokine receptor CXCR4-targeting probe ^{68}Ga-pentixafor. *J Nucl Med.* 2015;56:410–416.

30. Thackeray JT, Derlin T, Haghikia A, et al. Molecular imaging of the chemokine receptor CXCR4 after acute myocardial infarction. *JACC Cardiovasc Imaging.* 2015;8:1417–1426.

31. Heo GS, Kopecky B, Sultan D, et al. Molecular imaging visualizes recruitment of inflammatory monocytes and macrophages to the injured heart. *Circ Res.* 2019; 124:881–890.

32. English SJ, Sastriques SE, Detering L, et al. CCR2 positron emission tomography for the assessment of abdominal aortic aneurysm inflammation and rupture prediction. *Circ Cardiovasc Imaging.* 2020;13:e009889.

33. Liu Y, Pierce R, Luehmann HP, Sharp TL, Welch MJ. PET imaging of chemokine receptors in vascular injury–accelerated atherosclerosis. *J Nucl Med.* 2013;54:1135.

34. Dutta P, Sager Hendrik B, Stengel Kristy R, et al. Myocardial infarction activates CCR2+ hematopoietic stem and progenitor cells. *Cell Stem Cell.* 2015;16:477–487.

35. Razavian M, Tavakoli S, Zhang J, et al. Atherosclerosis plaque heterogeneity and response to therapy detected by in vivo molecular imaging of matrix metalloproteinase activation. *J Nucl Med.* 2011;52:1795–1802.

36. Su H, Spinale FG, Dobrucki LW, et al. Noninvasive targeted imaging of matrix metalloproteinase activation in a murine model of postinfarction remodeling. *Circulation.* 2005;112:3157–3167.

37. Fujimoto S, Hartung D, Ohshima S, et al. Molecular imaging of matrix metalloproteinase in atherosclerotic lesions: resolution with dietary modification and statin therapy. *J Am Coll Cardiol.* 2008;52:1847–1857.

38. Toczek J, Ye Y, Gona K, et al. Preclinical evaluation of RYM1, a matrix metalloproteinase-targeted tracer for imaging aneurysm. *J Nucl Med.* 2017;58:1318–1323.

39. Jung JJ, Razavian M, Challa AA, et al. Multimodality and molecular imaging of matrix metalloproteinase activation in calcific aortic valve disease. *J Nucl Med.* 2015;56:933–938.

40. Golestani R, Razavian M, Nie L, et al. Imaging vessel wall biology to predict outcome in abdominal aortic aneurysm. *Circ Cardiovasc Imaging.* 2014;8:e002471.

41. Razavian M, Nie L, Challa A, et al. Lipid lowering and imaging protease activation in atherosclerosis. *J Nucl Cardiol.* 2014;21:319–328.

42. Gona K, Toczek J, Ye Y, et al. Hydroxamate-based selective macrophage elastase (MMP-12) inhibitors and radiotracers for molecular imaging. *J Med Chem.* 2020; 63:15037–15049.

43. Laidlaw BJ, Craft JE, Kaech SM. The multifaceted role of CD4(+) T cells in CD8(+) T cell memory. *Nat Rev Immunol.* 2016;16:102–111.

44. Beckford Vera DR, Smith CC, Bixby LM, et al. Immuno-PET imaging of tumor-infiltrating lymphocytes using zirconium-89 radiolabeled anti-CD3 antibody in immune-competent mice bearing syngeneic tumors. *PLoS One.* 2018;13:e0193832.

45. Kristensen LK, Fröhlich C, Christensen C, et al. CD4(+) and CD8a(+) PET imaging predicts response to novel PD-1 checkpoint inhibitor: studies of Sym021 in syngeneic mouse cancer models. *Theranostics.* 2019;9:8221–8238.

46. Oliveira BL, Caravan P. Peptide-based fibrin-targeting probes for thrombus imaging. *Dalton Trans.* 2017;46:14488–14508.

47. Rezaeianpour S, Bozorgi AH, Moghimi A, et al. Synthesis and biological evaluation of cyclic [^{99m}Tc]-HYNIC-CGPRPPC as a fibrin-binding peptide for molecular imaging of thrombosis and its comparison with [^{99m}Tc]-HYNIC-GPRPP. *Mol Imaging Biol.* 2017;19:256–264.

48. Starmans LW, van Duijnhoven SM, Rossin R, et al. Evaluation of ^{111}In-labeled EPep and FibPep as tracers for fibrin SPECT imaging. *Mol Pharm.* 2013;10:4309–4321.

49. Blasi F, Oliveira BL, Rietz TA, et al. Multisite thrombus imaging and fibrin content estimation with a single whole-body PET scan in rats. *Arterioscler Thromb Vasc Biol.* 2015;35:2114–2121.

50. Izquierdo-Garcia D, Desogere P, Philip AL, et al. Detection and characterization of thrombosis in humans using fibrin-targeted positron emission tomography and magnetic resonance. *JACC Cardiovasc Imaging.* October 7, 2021 [Epub ahead of print].

51. Jamasbi J, Ayabe K, Goto S, Nieswandt B, Peter K, Siess W. Platelet receptors as therapeutic targets: past, present and future. *Thromb Haemost.* 2017;117:1249–1257.

52. Dunzinger A, Hafner F, Schaffler G, Piswanger-Soelkner JC, Brodmann M, Lipp RW. ^{99m}Tc-apcitide scintigraphy in patients with clinically suspected deep venous thrombosis and pulmonary embolism. *Eur J Nucl Med Mol Imaging.* 2008;35: 2082–2087.

53. Kim C, Lee JS, Han Y, et al. Glycoprotein IIb/IIIa receptor imaging with ^{18}F-GP1 positron emission tomography for acute venous thromboembolism: an open-label, non-randomized, first-in-human phase 1 study. *J Nucl Med.* 2018;60:244–249.

54. Chae SY, Kwon TW, Jin S, et al. A phase 1, first-in-human study of ^{18}F-GP1 positron emission tomography for imaging acute arterial thrombosis. *EJNMMI Res.* 2019;9:3.

55. Lohrke J, Siebeneicher H, Berger M, et al. ^{18}F-GP1, a novel PET tracer designed for high-sensitivity, low-background detection of thrombi. *J Nucl Med.* 2017;58: 1094–1099.

56. Hugenberg V, Zerna M, Berndt M, et al. GMP-compliant radiosynthesis of [^{18}F]GP1, a novel PET tracer for the detection of thrombi. *Pharmaceuticals (Basel).* 2021;14:739.

57. Reyes Gil M. Overview of the coagulation system. In: Shaz BH, Hillyer CD, Reyes Gil M, eds. *Transfusion Medicine and Hemostasis.* 3rd ed. Elsevier; 2019:559–564.

58. Andrews JPM, Portal C, Walton T, et al. Non-invasive in vivo imaging of acute thrombosis: development of a novel factor XIIIa radiotracer. *Eur Heart J Cardiovasc Imaging.* 2020;21:673–682.

59. Henderson NC, Rieder F, Wynn TA. Fibrosis: from mechanisms to medicines. *Nature.* 2020;587:555–566.

60. Soejima K, Stevenson WG. Ventricular tachycardia associated with myocardial infarct scar. *Circulation.* 2002;106:176–179.

61. Kwon DH, Hachamovitch R, Adeniyi A, et al. Myocardial scar burden predicts survival benefit with implantable cardioverter defibrillator implantation in patients with severe ischaemic cardiomyopathy: influence of gender. *Heart.* 2014;100:206.

62. Aljaroudi WA, Flamm SD, Saliba W, Wilkoff BL, Kwon D. Role of CMR imaging in risk stratification for sudden cardiac death. *JACC Cardiovasc Imaging.* 2013;6: 392–406.

63. Lan TH, Huang XQ, Tan HM. Vascular fibrosis in atherosclerosis. *Cardiovasc Pathol.* 2013;22:401–407.

64. McVicker BL, Bennett RG. Novel anti-fibrotic therapies. *Front Pharmacol.* 2017; 8:318.

65. Fitzgerald AA, Weiner LM. The role of fibroblast activation protein in health and malignancy. *Cancer Metastasis Rev.* 2020;39:783–803.

66. Varasteh Z, Mohanta S, Robu S, et al. Molecular imaging of fibroblast activity after myocardial infarction using a ^{68}Ga-labeled fibroblast activation protein inhibitor, FAPI-04. *J Nucl Med.* 2019;60:1743–1749.

67. Siebermair J, Köhler MI, Kupusovic J, et al. Cardiac fibroblast activation detected by Ga-68 FAPI PET imaging as a potential novel biomarker of cardiac injury/ remodeling. *J Nucl Cardiol.* 2021;28:812–821.

68. Heckmann MB, Reinhardt F, Finke D, et al. Relationship between cardiac fibroblast activation protein activity by positron emission tomography and cardiovascular disease. *Circ Cardiovasc Imaging.* 2020;13:e010628.

69. Wu M, Ning J, Li J, et al. Feasibility of in vivo imaging of fibroblast activation protein in human arterial walls. *J Nucl Med.* September 16, 2021 [Epub ahead of print].

70. Muzard J, Sarda-Mantel L, Loyau S, et al. Non-invasive molecular imaging of fibrosis using a collagen-targeted peptidomimetic of the platelet collagen receptor glycoprotein VI. *PLoS One.* 2009;4:e5585.

71. Velikyan I, Rosenström U, Bulenga TN, Eriksson O, Antoni G. Feasibility of multiple examinations using ^{68}Ga-labelled collagelin analogues: organ distribution in rat for extrapolation to human organ and whole-body radiation dosimetry. *Pharmaceuticals (Basel).* 2016;9:31.

72. Désogère P, Tapias LF, Rietz TA, et al. Optimization of a collagen-targeted PET probe for molecular imaging of pulmonary fibrosis. *J Nucl Med.* 2017;58:1991.

73. Montesi SB, Izquierdo-Garcia D, Désogère P, et al. Type I collagen-targeted positron emission tomography imaging in idiopathic pulmonary fibrosis: first-in-human studies. *Am J Respir Crit Care Med.* 2019;200:258–261.

74. Creager MD, Hohl T, Hutcheson JD, et al. ^{18}F-fluoride signal amplification identifies microcalcifications associated with atherosclerotic plaque instability in positron emission tomography/computed tomography images. *Circ Cardiovasc Imaging.* 2019;12:e007835.

75. Joshi NV, Vesey AT, Williams MC, et al. ^{18}F-fluoride positron emission tomography for identification of ruptured and high-risk coronary atherosclerotic plaques: a prospective clinical trial. *Lancet.* 2014;383:705–713.

76. Kwiecinski J, Tzolos E, Adamson PD, et al. Coronary ^{18}F-sodium fluoride uptake predicts outcomes in patients with coronary artery disease. *J Am Coll Cardiol.* 2020;75:3061–3074.

77. Jenkins WS, Vesey AT, Shah AS, et al. Valvular ^{18}F-fluoride and ^{18}F-fluorodeoxyglucose uptake predict disease progression and clinical outcome in patients with aortic stenosis. *J Am Coll Cardiol.* 2015;66:1200–1201.

78. Dweck MR, Jones C, Joshi NV, et al. Assessment of valvular calcification and inflammation by positron emission tomography in patients with aortic stenosis. *Circulation.* 2012;125:76–86.

79. Massera D, Trivieri MG, Andrews JPM, et al. Disease activity in mitral annular calcification. *Circ Cardiovasc Imaging.* 2019;12:e008513.

80. Tzolos E, Kwiecinski J, Berman D, Slomka P, Newby DE, Dweck MR. Latest advances in multimodality imaging of aortic stenosis. *J Nucl Med.* 2022;63:353–358.

81. Tzolos E, Dweck MR. ^{18}F-sodium fluoride (^{18}F-NaF) for imaging microcalcification activity in the cardiovascular system. *Arterioscler Thromb Vasc Biol.* 2020;40: 1620–1626.

82. Gillmore JD, Maurer MS, Falk RH, et al. Nonbiopsy diagnosis of cardiac transthyretin amyloidosis. *Circulation.* 2016;133:2404–2412.

83. Lee SP, Suh HY, Park S, et al. Pittsburgh B compound positron emission tomography in patients with AL cardiac amyloidosis. *J Am Coll Cardiol.* 2020;75:380–390.

84. Dorbala S, Vangala D, Semer J, et al. Imaging cardiac amyloidosis: a pilot study using ^{18}F-florbetapir positron emission tomography. *Eur J Nucl Med Mol Imaging.* 2014;41:1652–1662.

85. Kircher M, Ihne S, Brumberg J, et al. Detection of cardiac amyloidosis with ^{18}F-florbetaben-PET/CT in comparison to echocardiography, cardiac MRI and DPD-scintigraphy. *Eur J Nucl Med Mol Imaging.* 2019;46:1407–1416.

86. Papathanasiou M, Kessler L, Carpinteiro A, et al. ^{18}F-flutemetamol positron emission tomography in cardiac amyloidosis. *J Nucl Cardiol.* October 6, 2020 [Epub ahead of print].